Analyst

PAPER

View Article Online
View Journal

Cite this: DOI: 10.1039/d6an00127k

Quantitative analysis of sequential nucleic acid elution from silica paramagnetic beads

Asher Varon, [a] Justin Schares,[b] Kuangwen Hsieh,[a] Bradley Downs[c] and Tza-Huei Wang *[a,c,d]

Received 2nd February 2026,
Accepted 28th April 2026

DOI: 10.1039/d6an00127k

rsc.li/analyst

Paramagnetic bead–based capture and release is widely used for nucleic acid preparation in benchtop and automated workflows. In emerging magnetofluidic and cartridge-style point-of-care systems, sequential bead elution has only recently begun to be explored as a strategy to distribute limited nucleic acids across multiple reactions. In such designs, elution behavior becomes directly relevant to assay performance and multiplexing capacity. Here, we systematically examine multi-sequential elutions from silica paramagnetic beads and quantify each eluate by qPCR. We describe the data with a phenomenological, concentration-dependent, exponential-decay model and show that elution profiles depend on nucleic acid target size (soybean genomic DNA *versus* a short synthetic double-stranded DNA fragment, gBlock), starting concentration, and multiplexed (duplex) bead binding. We demonstrate reproducible nucleic acid signal across eight elutions, extract size-dependent decay constants, and evaluate model performance over a range of input concentrations. Duplex and alternating-trait experiments further show that the same framework can describe multi-target elution with limited data points per target. Together, these results provide a quantitative description of sequential nucleic acid elution from silica beads and a simple modeling approach that can inform the design of multi-step bead-based workflows.

Introduction

Magnetic beads have emerged as a versatile and mobile solid-phase carrier for nucleic acid (NA) preparation, enabling workflows from benchtop purification to automated sample processing and point-of-care (POC) diagnostics.[1–9] Over the past two decades, several studies have formalized the physical and chemical underpinnings of NA adsorption to paramagnetic silica beads, providing a framework for understanding the kinetics of target capture under varying binding conditions.[10–12] Follow-on work has refined this framework through computational modeling and direct physical characterization.[13–15] This has led to innovations such as chemically modifying bead surfaces for enhanced capture specificity or employing size-selective exclusion to control which NAs are retained.[16–18]

In contrast to the detailed study of capture, the release or elution process, particularly in a multi-sequential format, has been less systematically investigated. Early work noted that elution efficiency could vary with NA size, but offered little formal characterization for practical assay design.[19] More recent approaches have explored active control over elution, for example *via* electrically induced pH shifts or specialized micro-purification column geometries and flow regimes.[20,21] However, the potential to exploit an understanding of elution kinetics for predictable, programmable release of NAs across multiple elution steps remains largely untapped.

Our group and others have shown that silica bead-based elution can be performed sequentially, producing measurable yield in multiple rounds from the same bead pellet. We have explored this concept for automating complex NA workflows in multiplexed POC diagnostic formats for respiratory and sexually transmitted diseases.[22,23] Other studies have similarly demonstrated that environmental parameters such as elution temperature influence release profiles, suggesting equilibrium-based kinetic processes.[24–26] These findings hint at the possibility of using elution kinetics not only for purification but also for higher-order assay functions, such as partitioning targets across wells for parallel reactions or controlling which targets are released at each step. This capability is particularly relevant to multiplexed POC systems, where a limited sample may need to support several downstream amplification reactions. Although a single elution is generally sufficient when

[a]*Department of Mechanical Engineering, Johns Hopkins University, Baltimore, MD 21218, USA. E-mail: thwang@jhu.edu*
[b]*Corteva Agriscience, Johnston, IA 50131, USA*
[c]*Institute for NanoBiotechnology, Johns Hopkins University, Baltimore, MD 21218, USA*
[d]*Department of Biomedical Engineering, Johns Hopkins University, Baltimore, MD 21218, USA*

only one reaction is required, it does not by itself enable controlled allocation of NAs across multiple assays. In many current POC systems, multiplex testing is instead implemented by running multiple cartridges or by parallelizing sample preparation and reaction wells within a single cartridge. These approaches can require greater sample input and increase fluidic complexity along with extra valving steps that complicate automation.[27–29] Sequential bead elution provides an alternative that enables stepwise release of NAs without requiring additional splitting steps. Yet, key questions remain regarding the limits of elution efficiency, the maximum number of usable sequential elutions, and the roles of parameters such as NA target size (*e.g.*, genomic DNA *versus* short synthetic DNA fragments), starting concentration, and simultaneous multi-target binding.

These questions are increasingly relevant for emerging magnetofluidic and cartridge-based POC systems, where sequential bead elution has only recently begun to be explored as a strategy to distribute limited NA across multiple reactions.[22,30] In such designs, understanding how much NA is released at each elution, and how this depends on target size and loading, becomes directly linked to assay performance and multiplexing capacity. However, realizing this potential requires both empirical characterization of sequential elution and a simple modeling framework that can be used to predict elution behavior under different input conditions. Addressing these gaps is important for extending bead-based workflows beyond conventional NA extraction toward more programmable, multi-step architectures that are compatible with automated and POC implementations.

In this work, we systematically map the sequential elution behavior of silica paramagnetic beads under controlled conditions, using both soybean genomic DNA targets corresponding to specific traits and a short synthetic double-stranded DNA fragment (gBlock) as model systems. By holding elution time, temperature, and buffer composition constant, which are known to influence DNA release from silica paramagnetic beads, we isolate the effects of target size, input concentration, and duplexed binding on sequential elution behavior.[11,22] We then assess the predictive power of a phenomenological, concentration-dependent exponential-decay model to describe these behaviors. As a proof of concept, we demonstrate consistent deposition of detectable NA across eight elutions, the ability to duplex targets without losing predictable performance, and the feasibility of alternating target release patterns. Although our experiments are carried out with a single bead chemistry and a fixed elution protocol, the framework we develop is generic and can, in principle, be extended to other bead types and elution conditions in future studies. Together, these results expand the conceptual and practical boundaries of multi-sequential NA bead elution and lay the groundwork for programmable, multiplexed workflows that can inform the design of multi-step bead-based assays, including future magnetofluidic and POC implementations.

Methods and materials

Conceptual and experimental overview

This study was designed to test how NAs are progressively released from silica paramagnetic beads when the same bead preparation is subjected to multiple rounds of elution. Our goals were to define the practical limits of sequential recovery, identify the key factors that govern release efficiency, and evaluate whether elution behavior can be predicted by a simple kinetic model.

To address these questions, we compared elution profiles obtained from two classes of targets: complex biological soybean genomic DNA derived from seed lysate and short synthetic double-stranded DNA fragment (gBlock) (Fig. 1a). Soybean DNA was selected because it provides a high-molecular-weight template (~1.15 Gb) with well-characterized traits, enabling assessment of sequential elution efficiency across distinct loci and evaluation of target-specific effects while ensuring reproducible quantitative polymerase-chain reaction (qPCR) detection. The synthetic gBlock (~200 bp) was included as a complementary, small, defined target to examine size-dependent effects on release kinetics and provide a highly reproducible template. After binding and washing, each bead preparation was processed using a standardized magnetic capture and wash workflow (Fig. 1b). The same beads then underwent up to eight consecutive elution steps under constant thermal and buffer conditions, with each elution collected into fresh qPCR mix. The NA yield from each round was measured using real-time qPCR cycle quantification (C_q) values, enabling us to track depletion across elution cycles. Eight elutions were chosen to go beyond our prior investigation which investigated only up to three sequential elutions.[22] This approach allowed us to explore how far the depletion process could be extended while remaining practical for standard benchtop workflows. By holding environmental parameters such as elution temperature, incubation time, and buffer composition constant, we could isolate the influence of target size, input concentration, and duplexed binding. These data were then interpreted within an equilibrium-inspired framework to evaluate whether sequential elution follows predictable exponential decay patterns (Fig. 1c).

DNA preparation and dilution series preparation

Extraction was performed using a HotSHOT alkaline lysis buffer (sodium hydroxide with 1% sodium dodecyl sulfate). Crude DNA lysate was generated by combining 1.5 mL extraction buffer with 0.1 g ground soybean seed tissue. Immediately after extraction, 0.5 mL of potassium acetate precipitation buffer (pH 4.0) was added to precipitate SDS and inhibitors and reduce the overall pH to approximately 4.0. Prior to use, the lysate was passed through two 7 μm filters to remove precipitate.

For dilution experiments, a DNA-free control buffer ("blank buffer") was prepared by combining 1.5 mL extraction buffer and 0.5 mL precipitation buffer, followed by filtration. Soybean lysate samples were diluted using this blank buffer to generate

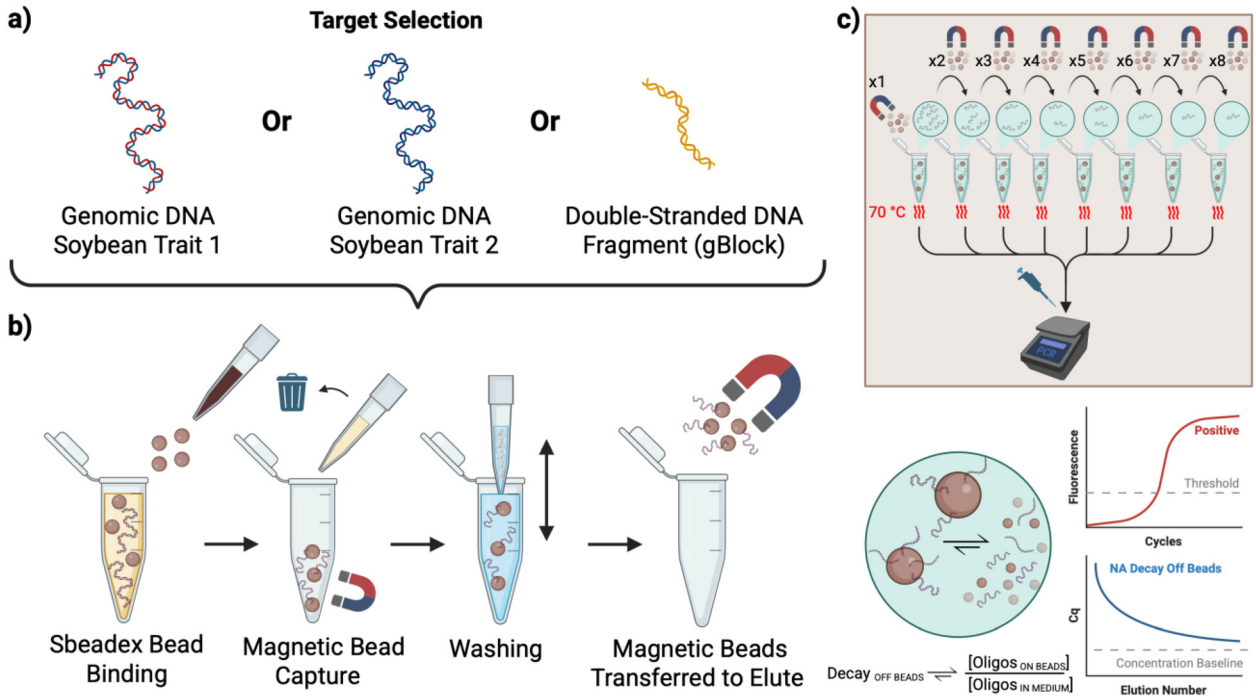

Fig. 1 Workflow for multi-sequential nucleic acid elution from silica paramagnetic beads. (a) Two classes of NA targets are used in this study: soybean genomic DNA derived from seed lysate corresponding to traits 1 and 2, and a short synthetic double-stranded DNA fragment (gBlock). (b) Sbeadex beads serve as the bead carrier, undergoing NA binding, magnetic bead recapture, and washing. (c) The washed beads undergo up to eight consecutive elution steps under constant conditions. In each step, beads are deposited into fresh qPCR mix and incubated at 70 °C for 2.5 min, after which the beads are transferred to the next elution well. From each elution, 5 μL of eluate is taken for qPCR. C_q values from all eight elutions are used to map NA release as a function of elution number.

relative input concentrations ranging from 100% to 10% of the original lysate in 10% increments, which were used to generate the model training dataset, with additional dilutions prepared at 1% and 0.1% for evaluation of low-level detection.

Synthetic double-stranded DNA (Integrated DNA Technologies) was diluted in TE buffer to a stock concentration of 20 000 copies per μL. Serial dilutions were then prepared in the relative input concentration form, ranging from 100% to 10% of the original stock concentration, with additional 1% and 0.1% dilutions for low-level evaluation. For consistency with crude soybean lysate samples and comparison across template types, these gBlock inputs are presented in the Results as relative percentages corresponding to fractions of the starting stock concentration.

qPCR setup and analysis

Assay targets were selected for two soybean traits ("trait 1" and "trait 2") and for the gBlock synthetic DNA. qPCR assay mixes were prepared using 5x PalmTaq Express Master Mix (Ahram Biosystems) and TaqMan NA assays (Life Technologies) to reach final concentrations of 1.25x PalmTaq mix and 1.25 μM TaqMan assay.

For each elution, 5.0 μL of sample was transferred into a 384-well plate for qPCR on a QuantStudio 7 Real-Time Thermocycler (Life Technologies). The qPCR protocol began with a hot start at 95 °C for 10 minutes, followed by 50 cycles of 95 °C for 10 seconds and 60 °C for 1 minute, with real-time fluorescent measurements taken at the end of each cycle. C_q values were automatically calculated using the QuantStudio 7 software with a relative threshold. These data were collected for subsequent modeling of NA elution.

To relate C_q values to template concentration, standard curves were generated for each assay. For soybean traits, qPCR assay mixes were prepared as above with the addition of genomic DNA at five sequential 1 : 5 dilutions (10.000 ng μL^{-1}, 2.000 ng μL^{-1}, 0.400 ng μL^{-1}, 0.080 ng μL^{-1}, and 0.016 ng μL^{-1}). For the gBlock template, five sequential 1 : 5 dilutions were also created using concentrations consistent with the genomic DNA units: 1.954×10^{-5} ng μL^{-1}, 3.907×10^{-6} ng μL^{-1}, 7.815×10^{-7} ng μL^{-1}, 1.563×10^{-7} ng μL^{-1}, and 3.126×10^{-8} ng μL^{-1}. Standard curves were run on the QuantStudio 7 using the same qPCR conditions, and the resulting plots were used to determine the relationship between C_q and NA concentration.

PCR efficiency for each assay was calculated from the slope of the standard curve using the formula: efficiency (%) = $(10^{-1/\text{slope}} - 1) \times 100$.

Sequential elution workflow

To probe the practical limits of sequential NA release, we implemented a multi-elution workflow instead of the conven-

tional single-elution protocol. In a 96-well plate, 100 μL of soybean seed lysate (or 105 μL gBlock sample in blank buffer) was mixed with 2.0 μL Sbeadex beads (LGC). Using a Kingfisher 96-well magnetic head (Thermo Scientific), beads were pelleted and transferred to a wash plate containing 100 μL ChargeSwitch wash solution (Thermo Scientific) overlaid with 60 μL silicone oil (MicroLubrol).

After washing, beads were transferred into a fresh plate containing 10 μL qPCR mix (also overlaid with 100 μL silicone oil) and incubated on a thermocycler block (Bio-Rad) at 70 °C for 2.5 min to elute NAs. Unlike traditional workflows where eluates are collected once for downstream use, the magnetic head was reapplied to pellet and transfer the same beads into a fresh well containing new qPCR mix for each subsequent elution. This cycle was repeated eight times to capture depletion kinetics beyond the previously reported three-elution limit while maintaining a practical plate footprint.

All environmental parameters, including temperature, incubation time, and buffer composition, were held constant across runs to ensure that observed differences in elution profiles reflected only target size, starting concentration, or duplexing effects. After the eighth elution, beads were removed and discarded.

Sequential elution modeling and data analysis

Elution of NAs from silica substrates has commonly been modeled using equilibrium-based approaches. A common example is the Langmuir isotherm, which assumes reversible adsorption to a finite number of surface sites and predicts desorption based on the concentration gradient between bound and free states.[31–33] In practice, this has often been approximated with first-order models, which assume that a constant fraction of the remaining bound material is released at each step.[34] While mathematically convenient, these models rely on assumptions such as uniform binding affinity, rapid equilibration, and negligible influence of initial loading on release dynamics.

In our system, we hypothesize that NA release is governed by both thermodynamic (concentration gradient–driven) and kinetic (rate-limited) factors and that simple fixed-fraction models may not fully capture the observed dependence on initial loading. Accordingly, we adopted a phenomenological, concentration-dependent exponential-decay model that we chose for its simplicity, empirical fit quality, and interpretability rather than as a strict mechanistic derivation from first principles. We note that simpler models (for example, a single-parameter exponential decay as a function of elution number) can qualitatively describe the monotonic decrease in signal, but preliminary comparisons indicated that these models did not capture the concentration dependence as effectively as the form used here.

We represent the amount of NA eluted at each step as a concentration-weighted exponential decay:

$$E_N = (a_1 z + a_0) \cdot e^{-kN} \quad (1)$$

where N is the elution step number, k is the elution decay constant (1/elution step), $z = \log_{10}(NA_0)$ is the log-transformed initial sample concentration, a_1 and a_0 are parameters that determine how input concentration influence total NA available for elution. qPCR provides a C_q value inversely related to the logarithm of the eluate concentration, which we modeled as:

$$C_q = c_0 - \beta \log_{10}(E_N) \quad (2)$$

where β and c_0 are the slope and intercept from the qPCR standard curve, respectively. To allow for a concentration-dependent baseline shift in C_q values (*e.g.* background amplification or residual signal), we extend the model as follows:

$$C_q(N) = (a_1 z + a_0) \cdot e^{-kN} + (b_1 z + b_0) \quad (3)$$

Model parameters (a_0, a_1, b_0, b_1) were fit by nonlinear least squares regression of C_q values across elution steps and input concentrations and were plotted and analyzed using MATLAB R2018 (MathWorks, MA, USA).

Results and discussion

Training dataset and exponential decay model

We first qualitatively examined the elution behavior for soybean genomic DNA targets and for the small synthetic gBlock at undiluted sample concentrations. For both soybean traits (trait 1 and trait 2) and the synthetic DNA target, C_q signals were obtained for all eight elutions (Fig. 2a–c). We then quantitatively assessed these elution profiles using our hypothesized model (see Methods and materials). Training sets of eight sequential elutions, comprising sample concentrations between 20% and 100% of initial soybean genomic DNA lysates (for traits 1 and 2) and, similarly, between 20% and 100% of the starting stock for the small synthetic DNA target were compiled. The general model was fit to each concentration in the training sets using nonlinear least squares regression to determine the kinetic and concentration-dependent parameters. As defined in eqn (3), we expected the fitted parameters to capture both the concentration dependence and the rate constant (Fig. S1–S3).

Overall, the model provided strong fits for each training set, with R^2 values ranging from 0.94 to 1.00. We observed C_q variability among replicates for a given concentration, occasionally as large as $2.2C_q$, which may have reflected minor experimental variability such as incomplete bead transfer or slight differences in initial binding efficiency. However, the overall trend remained consistent, supporting the reliability of the decay constants. To reduce variability and obtain more stable estimates for each target, we averaged constants across the training sets, yielding an exponential decay constant k = 0.41 per elution for soybean genomic DNA trait 1, k = 0.46 per elution for soybean genomic DNA trait 2, and k = 0.31 per elution for the small synthetic DNA target (gBlock). Larger k values indicated more rapid depletion of NA from the beads across sequential elutions; thus, the genomic DNA traits depleted more quickly per elution step than the smaller gBlock fragment under these conditions, likely reflecting

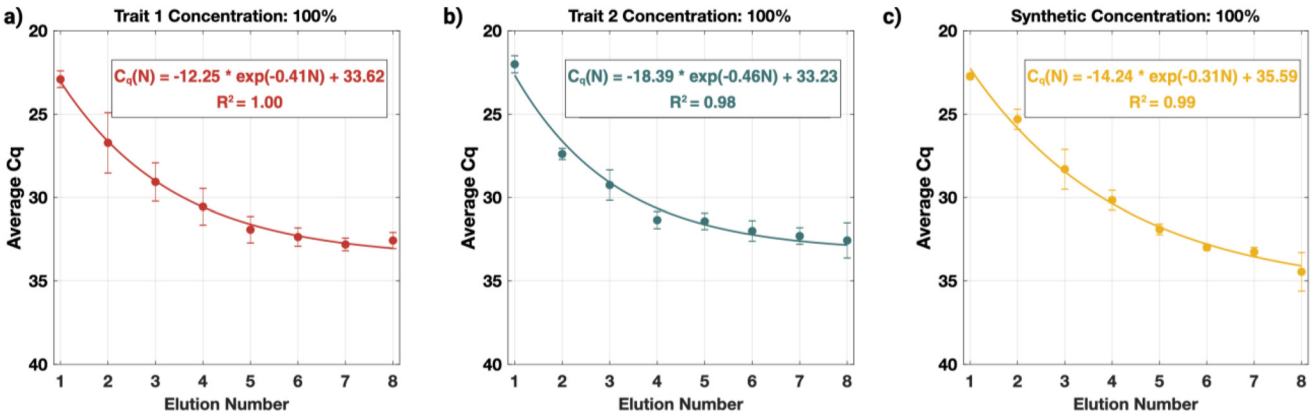

Fig. 2 Elution model fits for training samples. Average C_q values ± standard deviation are fit with the concentration-dependent exponential decay model. (a) Soybean genomic DNA trait 1 is fit to the model with an exponential decay constant k = 0.41 per elution. (b) Soybean genomic DNA trait 2 is fit to the model k = 0.46C_q per elution. (c) Small synthetic DNA target (gBlock) is fit to the model k = 0.31 per elution. All samples are measured at undiluted (100%) lysate or target concentration; data represent mean ± SD from triplicate experiments (n = 3). Note: The y-axis is inverted to reflect the inverse relationship between qPCR C_q values and the logarithmic nature of the eluted NAs, such that higher C_q values correspond to lower NA amounts.

differences in binding site accessibility or bead-surface interactions.

We expected the two soybean genomic DNA traits to exhibit similar decay constants, and the shorter synthetic DNA target to exhibit a different one. To statistically test these differences, we performed a nonparametric Kruskal–Wallis test followed by Dunn's multiple comparisons on the non-averaged decay constants from each training set. As anticipated, there was no significant difference between soybean genomic DNA traits 1 and 2 (adjusted p-value = 1.0000), whereas statistically significant differences were observed between the small synthetic DNA target (gBlock) and the soybean genomic DNA targets for both traits (adjusted p-values 0.03785 and 0.004022) (Fig. S4). These results confirmed that NA target size influenced sequential elution kinetics and, therefore, provide a quantitative basis for predicting depletion behavior in multi-step workflows.

Validation dataset and concentration dependency

Next, we generated independent validation datasets using 10-fold dilution series from 10% to 0.1% for each starting target stock to identify the minimal concentration at which DNA targets could be reliably detected across all elutions (Fig. 3a–c). For all targets and target types, 10% and 1% input concentrations exhibited strong model performance, with C_q signal in all eight elutions and R^2 values above 0.9.

To further assess model fidelity, we computed 95% confidence intervals for each fit and observed that model uncertainty increased as concentration decreased from 10% to 1%, particularly for soybean genomic DNA trait 2 and the small synthetic DNA target (gBlock). We also observed deviations from simple exponential decay beyond elution six, with some samples showing decreased C_q values (*i.e.*, higher apparent nucleic release) at later elutions. Two factors likely contributed to these observations. First, qPCR efficiency variations could have introduced greater C_q scatter among replicates at low template levels (Fig. S5). Second, NA elutions may have become unstable beyond certain low elution concentrations, and qPCR thresholding might not have accurately quantified signal once the eluted amount approached the detection limit.

These trends were even more pronounced at 0.1% input concentrations. For soybean genomic DNA trait 1 and the small synthetic DNA target, R^2 values decreased to 0.78 and 0.75, respectively. For trait 1, C_q could not be determined for elution eight and was therefore excluded from the fit. For soybean genomic DNA trait 2, the overall R^2 remained high (0.99), but undeterminable C_qs for elutions seven and eight raised questions about the reliability of those late-elution data points. For the small synthetic DNA target, C_qs were obtained for all eight elutions, but with increased scatter. While additional work is needed to fully understand NA behavior at these lower concentrations, these data suggested that at sufficiently low input levels, differences in NA target size (genomic DNA *versus* a short synthetic double-stranded DNA fragment) may become a dominant factor in elution kinetics relative to concentration. Together, these findings illustrate that decay constants not only reflect depletion kinetics at higher concentrations but also provide practical guidance for planning sequential elutions at low input levels, particularly for low-abundance targets or multiplexed samples, where late elutions may approach detection limits.

Target duplexing and trait patterning

We next asked whether simultaneous bead binding and elution of multiple targets would affect elution characteristics. To probe this, we employed duplex bead binding and elution using soybean genomic DNA trait 1 and the small synthetic DNA target (gBlock). Following elution, we carried out duplex qPCR on each eluate across all eight elution steps and applied our model to the resulting C_q values.

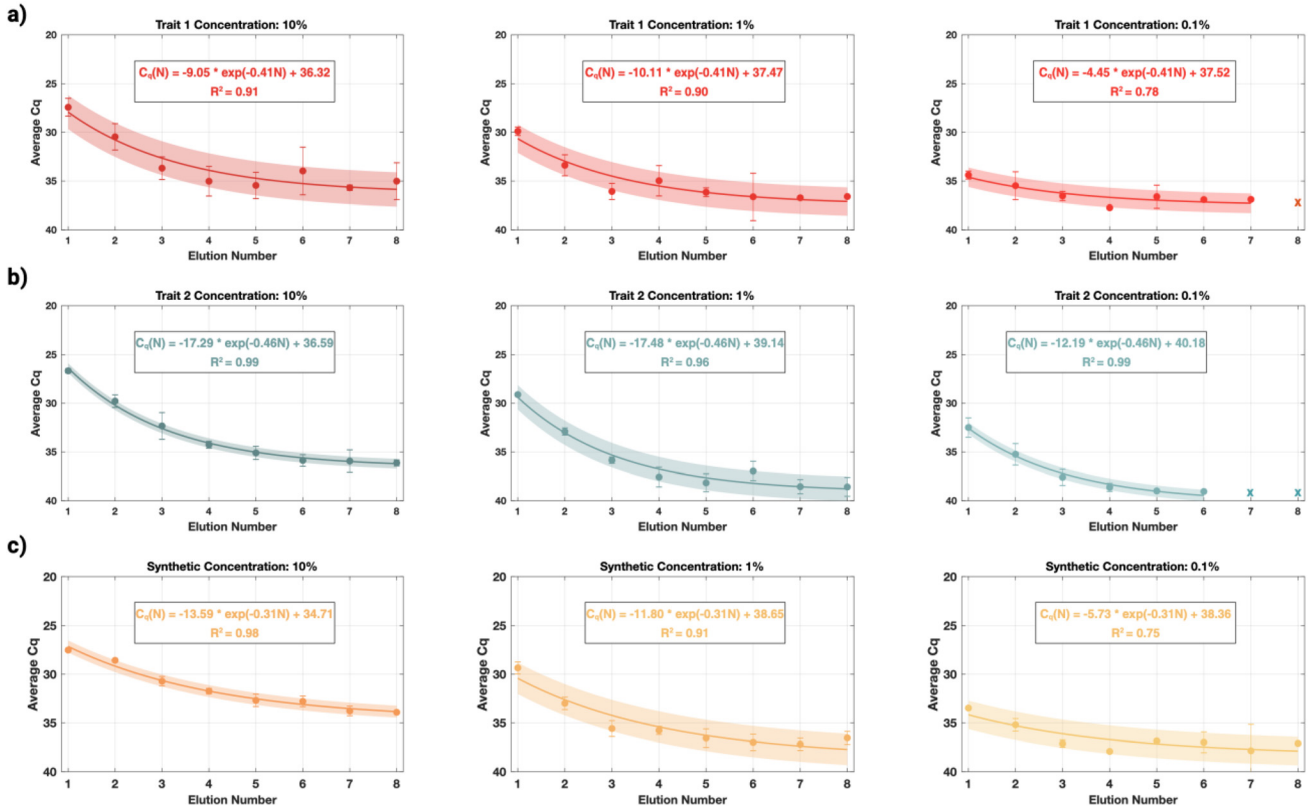

Fig. 3 Validation of the elution model across input concentrations. Model fits for 10%, 1%, and 0.1% input concentrations are shown with 95% confidence intervals. (a) Soybean genomic DNA trait 1 at 10%, 1%, and 0.1% lysate concentrations is fit to the model. (b) Soybean genomic DNA trait 2 at 10%, 1%, and 0.1% lysate concentrations is fit to the model. (c) Small synthetic DNA target (gBlock) at 10%, 1%, and 0.1% equivalent input concentrations is fit to the model. Elution steps with undeterminable C_q values are marked with an "*x*" and are excluded from the model fits. Data represent mean ± SD from replicate experiments (n = 3).

Elution profiles for both targets qualitatively resembled those observed when each NA was tested alone at full concentration (Fig. 4a). Model assessment showed strong fits, with R^2 values of 0.97 for both NAs. Although fluorescent signal was detected for all elutions, we observed a decrease in C_q between elutions six and seven for both targets, similar to the behavior discussed earlier in the validation experiments, which may indicate an approximate limit for accurate C_q quantification under our conditions. Differences in qPCR efficiency between the two assays in the duplex reaction (Fig. S6) could also have contributed to these apparent limits. Further optimization of the duplex qPCR to harmonize qPCR efficiencies would therefore be warranted for more detailed kinetic analysis. Nonetheless, the relatively strong fits obtained for the duplexed targets highlight the robustness of the model, indicating that the presence of a second target does not substantially alter the depletion kinetics of either NA. This suggests that sequential elution can maintain predictable release profiles even in multiplexed conditions and raises interesting questions for future work regarding how multiplexed targets of different NA sizes influence bead elution kinetics.

Finally, we sought to demonstrate that more complex samples could produce predictable elution patterns, even when only limited detection data are available. As a proof of concept, all three targets, both genomic DNA traits and the small synthetic DNA, were eluted in every well across eight sequential elutions, with the synthetic DNA detected in every elution and the genomic traits detected alternately (Fig. 4b). For the small synthetic DNA target, the model again displayed a strong fit (R^2 = 0.92), similar to our other duplexed experiments, with minor C_q variation observed at later elutions. Because only four elutions were allocated to each soybean genomic DNA trait, model fits were based on four data points per trait. Even with this limited dataset, the model achieved strong fits, with R^2 values of 0.99 and 0.95 for traits 1 and 2, respectively. These findings indicated that the model could reliably capture elution kinetics even in staggered or limited-data scenarios, supporting the quantitative application of sequential elution to multiplexed and alternating-target assay designs. Thus, this provides a framework for rationally designing multi-step workflows that distribute multiple targets across wells, while maintaining predictable performance. Such strategies could be leveraged in the future for semi-quantitative comparisons of genomic biomarkers, improving quantification accuracy, or normalizing elution quantification between reference and biomarker targets.

These results also clarify how the experimentally determined decay constant, k, can be applied across a range of experimental designs. Across varying input concentrations and

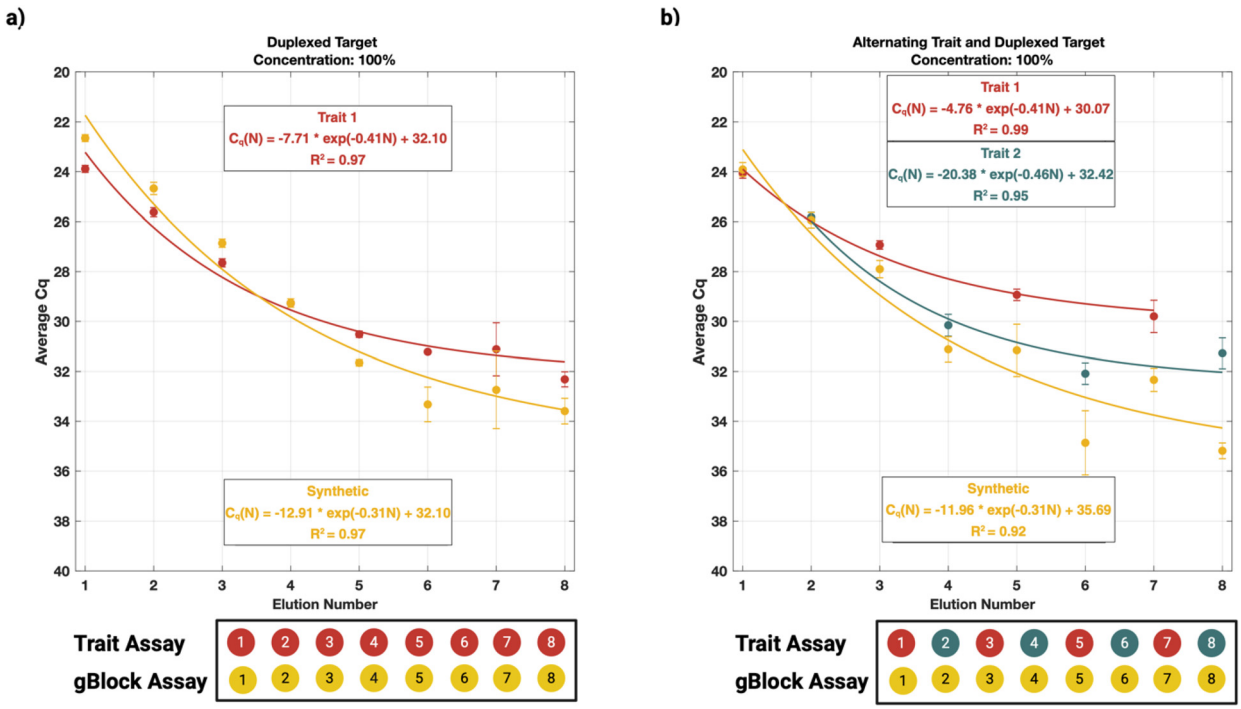

Fig. 4 Duplexed target binding and elution. (a) Duplex bead binding and elution of soybean genomic DNA trait 1 (red) and the small synthetic DNA target gBlock (yellow) across all eight elution wells, with each target fit using its specific elution model. Targets were quantified using a duplex qPCR assay in which both targets were measured in each elution well. The colored circles beneath the plot indicate the presence of trait 1 and gBlock in each numbered elution well. (b) Alternating elution pattern in which soybean genomic DNA trait 1 (red) and trait 2 (blue) are alternated across the eight elution wells, while the small synthetic DNA target gBlock (yellow) is present in every elution. The colored circles beneath the plot indicate which targets are present in each numbered elution well. Each soybean genomic DNA trait is fit using four data points (four elutions per trait), and the gBlock target is fit using eight data points (all eight elutions), demonstrating that the model remains robust even with limited elution data for individual traits. Data represent mean ± SD from replicate experiments (n = 3).

multiplexed conditions, k remained consistent, indicating that it primarily reflects the interaction between a given NA target and the bead-based binding and elution process rather than the presence of additional targets. This interpretation assumes that the bead surface is neither strongly saturated nor severely undersaturated and that bead chemistries interact with NAs through similar physical binding mechanisms.

Under these controlled conditions, the decay constant can be established once and then used to guide sequential elution workflows as a quantitative parameter describing elution behavior without needing to refit the model for each experiment. Thus, the same k value can be applied when the following conditions are maintained: (i) the same bead chemistry and binding mechanism; (ii) the same elution protocol; (iii) similar NA target characteristics (*e.g.*, fragment size or structure); and (iv) comparable qPCR assay conditions. Under these conditions, input concentration primarily affects signal magnitude but not the underlying depletion kinetics.

Conclusion

In this study, we systematically investigated sequential elution of nucleic acids from silica paramagnetic beads, evaluating how release depends on target size, input concentration, and multiplexed binding. Using soybean genomic DNA and a small synthetic gBlock fragment, we demonstrated measurable recovery across up to eight sequential elutions. A concentration-dependent exponential-decay model captured the observed elution kinetics with high fidelity, revealing size-dependent behavior, with smaller fragments exhibiting distinct elution decay from larger genomic targets. Duplexed and patterned multi-target experiments showed that predictable elution behavior can be maintained even under complex target conditions, supporting the use of sequential bead elution for controlled partitioning and multiplexing across wells.

Validation across a range of input concentrations showed that the model remained robust at higher and intermediate template levels, while late elutions at low concentrations were semi-quantitative, reflecting qPCR limits and increased sensitivity to small variations in handling. This highlights the practical constraints of sequential elution and should inform experimental design for both single and multi-target applications.

Our present experiments are limited to a single silica bead chemistry (Sbeadex) and a fixed elution protocol, and we therefore constrain our conclusions to these conditions. Nonetheless, the empirical modeling approach we describe is

general and could be applied to other bead types, buffer systems, and elution schedules to extract analogous kinetic parameters. Quantifying the fraction of nucleic acid released at each step provides a basis for designing multi-step workflows in which a single bead pellet is moved through multiple reaction chambers.

Given the current landscape of magnetofluidic and bead-based systems, sequential bead elution is particularly well suited for integration into compact, portable, POC diagnostic platforms.[35–37] Although full POC implementation was not explored in this study, we envision that future work could leverage magnetic actuation to transport bead pellets through simply designed POC cartridges. These cartridges could include additional reaction chambers to enable stepwise NA release, reducing fluidic complexity and eliminating the need for extra pumps or manual pipetting. By identifying the key parameters that govern sequential elution and establishing a straightforward kinetic framework, this work expands the utility of bead-based systems beyond conventional NA extraction toward programmable, multiplexed, and potentially POC applications.

Author contributions

A. Varon: conceptualization, investigation, methodology, formal analysis, writing – original draft, writing – review & editing, visualization. Justin Schares: experiment design and investigation, data curation, writing – review & editing, resources. K. Hsieh: formal analysis, writing – original draft, writing – review & editing, supervision. B. Downs: conceptualization, writing – review & editing. T. H. Wang: conceptualization, writing – review & editing, supervision, funding acquisition.

Conflicts of interest

The authors declare no competing financial interest.

Data availability

All data supporting the findings of this study are included in the article and its supplementary information (SI). Supplementary information: raw data used in compiling model training sets in demonstrated (Fig. S1–S3), followed by underlying statistical (Fig. S4) and assay assumptions (Fig. S5 and S6). See DOI: https://doi.org/10.1039/d6an00127k.

The raw datasets and analysis code generated or used in this study are available from the corresponding author upon reasonable request.

Acknowledgements

This research is financially supported by the National Institutes of Health (R01AI183336 and R01AI181217) and a collaboration research grant sponsored by Corteva Agriscience (TRAC20359). Some figures and figure layouts in this work were created with BioRender.com.

ChatGPT-5 (OpenAI) was employed to assist in manuscript text editing and the logical structure of data analysis code. The original manuscript text, insights, data modeling, and conclusions is the sole work of the authors.

References

1 S. I. Pearlman, M. Leelawong, K. A. Richardson, N. M. Adams, P. K. Russ, M. E. Pask, A. E. Wolfe, C. Wessely and F. R. Haselton, *ACS Appl. Mater. Interfaces*, 2020, **12**, 12457–12467, DOI: 10.1021/acsami.9b21564.
2 P. Li, M. Li, D. Yue and H. Chen, *J. Sep. Sci.*, 2022, **45**, 172–184, DOI: 10.1002/jssc.202100295.
3 A. J. Politza, T. Liu and W. Guan, *Lab Chip*, 2023, **23**, 3882–3892, DOI: 10.1039/D3LC00545C.
4 W. Yu, H. Lin, Y. Wang, X. He, N. Chen, K. Sun, D. Lo, B. Cheng, C. Yeung, J. Tan, D. D. Carlo and S. Emaminejad, *Sci. Robot*, 2020, **5**(39), DOI: 10.1126/scirobotics.aba4411.
5 Y. Zhang and T. Wang, *Adv. Mater.*, 2013, **25**, 2903–2908, DOI: 10.1002/adma.201300383.
6 W. H. Henley, N. A. Siegfried and J. M. Ramsey, *Lab Chip*, 2020, **20**, 1771–1779, DOI: 10.1039/D0LC00069H.
7 D. E. Gaddes, P. Lee, A. Y. Trick, P. Athamanolap, C. M. O'Keefe, C. Puleo, K. Hsieh and T. Wang, *Anal. Chem.*, 2020, **92**, 13254–13261, DOI: 10.1021/acs.analchem.0c02454.
8 F. Chen, J. Wang, A. H. Nambiar, J. Hardick, J. Melendez, A. Y. Trick and T. Wang, *ACS Sens.*, 2023, **8**, 1550–1557, DOI: 10.1021/acssensors.2c02630.
9 A. G. Ayers, C. M. Victoriano and S. K. Sia, *Lab Chip*, 2024, **24**, 5124–5136, DOI: 10.1039/D4LC00571F.
10 T. H. Nguyen and M. Elimelech, *Biomacromolecules*, 2007, **8**, 24–32, DOI: 10.1021/bm0603948.
11 P. E. Vandeventer, J. S. Lin, T. J. Zwang, A. Nadim, M. S. Johal and A. Niemz, *J. Phys. Chem. B*, 2012, **116**, 5661–5670, DOI: 10.1021/jp3017776.
12 P. E. Vandeventer, J. Mejia, A. Nadim, M. S. Johal and A. Niemz, *J. Phys. Chem. B*, 2013, **117**, 10742–10749, DOI: 10.1021/jp405753m.
13 B. Shi, Y. K. Shin, A. A. Hassanali and S. J. Singer, *J. Phys. Chem. B*, 2015, **119**, 11030–11040, DOI: 10.1021/acs.jpcb.5b01983.
14 C. Katevatis, A. Fan and C. M. Klapperich, *PLoS One*, 2017, **12**, e0176848, DOI: 10.1371/journal.pone.0176848.
15 J. Yang, Q. Su, C. Song, H. Luo, H. Jiang, M. Ni and F. Meng, *Phys. Chem. Chem. Phys.*, 2024, **26**, 22681–22695, DOI: 10.1039/D4CP02260B.
16 S. Rödiger, C. Liebsch, C. Schmidt, W. Lehmann, U. Resch-Genger, U. Schedler and P. Schierack, *Microchim. Acta*, 2014, **181**, 1151–1168, DOI: 10.1007/s00604-014-1243-4.

17 K. E. Sapsford, W. R. Algar, L. Berti, K. B. Gemmill, B. J. Casey, E. Oh, M. H. Stewart and I. L. Medintz, *Chem. Rev.*, 2013, **113**, 1904–2074, DOI: 10.1021/cr300143v.
18 X. Wang, L. Zhao, X. Wu, H. Luo, D. Wu, M. Zhang, J. Zhang, M. Pakvasa, W. Wagstaff, F. He, Y. Mao, Y. Zhang, C. Niu, M. Wu, X. Zhao, H. Wang, L. Huang, D. Shi, Q. Liu, N. Ni, K. Fu, K. Hynes, J. Strelzow, M. E. Dafrawy, T. He, H. Qi and Z. Zeng, *Genes Dis.*, 2021, **8**(3), 298–306, DOI: 10.1016/j.gendis.2020.04.013.
19 R. Kaur, R. Kumar and A. K. Bachhawat, *Nucleic Acids Res.*, 1995, **23**, 4932–4933, DOI: 10.1093/nar/23.23.4932.
20 T. Geng, N. Bao, O. Z. Gall and C. Lu, *Chem. Commun.*, 2009, 800–802, DOI: 10.1039/B817034G.
21 T. Poeckh, S. Lopez, A. O. Fuller, M. J. Solomon and R. G. Larson, *Anal. Biochem.*, 2008, **373**, 253–262, DOI: 10.1016/j.ab.2007.10.026.
22 A. Y. Trick, F. Chen, L. Chen, P. Lee, A. C. Hasnain, H. H. Mostafa, K. C. Carroll and T. Wang, *Adv. Mater. Technol.*, 2022, **7**(6), DOI: 10.1002/admt.202101013.
23 A. Y. Trick, J. H. Melendez, F. Chen, L. Chen, A. Onzia, A. Zawedde, E. Nakku-Joloba, P. Kyambadde, E. Mande, J. Matovu, M. Atuheirwe, R. Kwizera, E. A. Gilliams, Y. Hsieh, C. A. Gaydos, Y. C. Manabe, M. M. Hamill and T. Wang, *Sci. Transl. Med.*, 2021, **13**(593), DOI: 10.1126/scitranslmed.abf6356.
24 X. Li, J. Zhang and H. Gu, *Langmuir*, 2011, **27**, 6099–6106, DOI: 10.1021/la104653s.
25 K. A. Melzak, C. S. Sherwood, R. F. B. Turner and C. A. Haynes, *J. Colloid Interface Sci.*, 1996, **181**, 635–644, DOI: 10.1006/jcis.1996.0421.
26 M. A. Winters, J. D. Richter, S. L. Sagar, A. L. Lee and R. J. Lander, *Biotechnol. Prog.*, 2003, **19**, 440–447, DOI: 10.1021/bp020043e.
27 A. C. Hasnain, A. Stark, A. Y. Trick, K. Ma, K. Hsieh, Y. Cheng, S. J. Meltzer and T. Wang, *ACS Nano*, 2024, **18**, 12105–12116, DOI: 10.1021/acsnano.3c10070.
28 T. Zhou, N. Li, D. Chen and J. Wang, *Sens. Actuators, B*, 2025, **442**, 138139, DOI: 10.1016/j.snb.2025.138139.
29 D. S. Juang, T. D. Juang, D. M. Dudley, C. M. Newman, M. A. Accola, W. M. Rehrauer, T. C. Friedrich, D. H. O'Connor and D. J. Beebe, *Nat. Commun.*, 2021, **12**(1), DOI: 10.1038/s41467-021-24463-4.
30 A. S. De Olazarra, F. Chen, T. Wang and S. X. Wang, *ACS Sens.*, 2023, **8**, 2780–2790, DOI: 10.1021/acssensors.3c00696.
31 J. L. Steinbacher and C. C. Landry, *Langmuir*, 2014, **30**, 4396–4405, DOI: 10.1021/la402850m.
32 Q. Yuan, Z. Liang, S. Wang, P. Zuo, Y. Wang and Y. Luo, *Colloids Surf., A*, 2022, **644**, DOI: 10.1016/j.colsurfa.2022.128831.
33 S. M. Lorena, P. C. Cynthia, A. R. M. Isabela, V. M. Pamela, R. H. Gabriela, B. Jorge and G. Mariano, *Sep. Purif. Rev.*, 2023, **52**, 193–204, DOI: 10.1080/15422119.2022.2053159.
34 S. Bag, S. Rauwolf, S. P. Schwaminger, W. Wenzel and S. Berensmeier, *Langmuir*, 2021, **37**, 5902–5908, DOI: 10.1021/acs.langmuir.1c00381.
35 H. Lin, W. Yu, K. A. Sabet, M. Bogumil, Y. Zhao, J. Hambalek, S. Lin, S. Chandrasekaran, O. Garner, D. D. Carlo and S. Emaminejad, *Nature*, 2022, **611**, 570–577, DOI: 10.1038/s41586-022-05408-3.
36 J. Cheong, H. Yu, C. Y. Lee, J. Lee, H. Choi, J. Lee, H. Lee and J. Cheon, *Nat. Biomed. Eng.*, 2020, **4**, 1159–1167, DOI: 10.1038/s41551-020-00654-0.
37 T. Liu, G. Choi, Z. Tang, A. Kshirsagar, A. J. Politza and W. Guan, *Biosens. Bioelectron.*, 2022, **209**, DOI: 10.1016/j.bios.2022.114255.